Revista Mexicana de Astronomía y Astrofísica, **51**, 119–131 (2015)

ON THE EQUILIBRIUM OF A DISTORTED HETEROGENEOUS ELLIPSOIDAL MASS. I. THE HOMOGENEOUS MASS

J. U. Cisneros Parra,[1] F. J. Martínez Herrera,[2] and J. D. Montalvo Castro[2]

Received January 27 2015; accepted February 12 2015

RESUMEN

Partiendo de una ecuación monoparamétrica de cuarto orden para la superficie de un elipsoide (en vez de segundo orden, como en las clásicas figuras homogéneas), se investiga el equilibrio hidrostático de una masa heterogénea, cuya versión homogénea -que será la única que abordemos en el presente artículo- guarda un parecido con un elipsoide de Jacobi, salvo que la nuestra es estática, siendo un movimiento de vorticidad diferencial el que establece su equilibrio. La serie de Jacobi, que es *completa*, resulta ser un caso particular de las nuestras, las cuales están truncadas por el valor del parámetro en la ecuación de la superficie, que asimismo determina si la velocidad angular crece paulatinamente del ecuador al polo, o viceversa; o si es entre ellos donde alcanza su valor máximo. El modelo esferoidal -nuestra versión de un esferoide de Maclaurin- se trata como un caso particular del elipsoidal.

ABSTRACT

Departing from a mono-parametric fourth-order surface equation for an ellipsoid (rather than of the second order, as in the classical homogeneous figures), we investigate the hydrostatic equilibrium of a heterogeneous mass, whose homogeneous version—which will be the only one considered in the current paper—resembles a Jacobi ellipsoid, with the proviso that ours is static, its equilibrium being established by a differential vorticity motion. The Jacobi series, which is *complete*, turns out to be a particular case of ours, which are truncated by the value of the surface equation parameter, that further determines if the angular velocity steadily increases from the equator to the pole, or vice versa; or if it has a maximum value between them. The spheroidal model—our version of a Maclaurin spheroid—is treated as a particular case of the ellipsoidal one.

Key Words: gravitation — hydrodynamics — stars: rotation

1. INTRODUCTION

In past works, we were engaged with the question of equilibrium and stability of an inhomogeneous body, held together by gravitational attraction, consisting of two confocal, either spheroids or ellipsoids, that we called the *nucleus* and the *atmosphere* with, as in real stars, the nucleus being denser than the atmosphere. Our aim was to gain some physical insight on what comes about in celestial rotating bodies, imitating them in a coarse way—our model is composed of an ideal, incompressible fluid—by using analytical descriptions (like the ellipsoid equation) rather than pure numerical procedures.

We may summarize our past results as follows. For spheroids, no figures result when the nucleus and the atmosphere rotate with common and constant angular velocity; on the other hand, a series of oblate figures arises when the nucleus is flatter and rotates faster than the atmosphere (Cisneros et al. 1983). For ellipsoids, no figures were found in the case of common and constant angular velocity; anyway, these configurations—as we

[1]Facultad de Ciencias, Universidad Autónoma de San Luis Potosí, Mexico.
[2]Instituto de Física, Universidad Autónoma de San Luis Potosí, Mexico.

became aware afterwards—are ruled out by Hamy's theorem (Hamy 1887; Tassoul 1978); the case of different angular velocities was rejected beforehand, because the velocity fields of the nucleus and the atmosphere are likely to interfere destructively with each other.

Admitting Hamy's theorem, we pursued the ellipsoidal model idea after noticing that, among the members of the inhomogeneous spheroids series quoted above, there were some having a neutral frequency, which encouraged us to inquire if, by analogy with the homogeneous figures, tri-axial figures could branch off (bifurcate) from them.

To this end, a Riemann-type model of class S was employed, in which the nucleus and the atmosphere, while rotating with a common angular velocity, are endowed with internal currents of different vorticity. Although this model contributes figures (Cisneros et al. 1993, 2000, 2004), their accuracy is far from matching that of the classical homogeneous ones; furthermore, none of them can simultaneously be fully ellipsoidal in both nucleus *and* atmosphere, unless the last is but a very thin shell, i.e., when the figures are nearly homogeneous. Clearly, any further pretension of looking for heterogeneous ellipsoidal figures, without sacrificing accuracy, compels us to take distance from the standard ellipsoid quadratic equation.

2. OUR MODEL

Our new model is constructed on the base of a distorted ellipsoid, whose surface equation is

$$\frac{x^2}{a_1^2}+\frac{y^2}{a_2^2}+\frac{z^2}{a_3^2}+d\,\frac{z^4}{a_3^4}=1, \tag{1}$$

so that tri-planar symmetry is preserved and the transverse sections are again ellipses; d is a parameter independent of x, y and z; a_1 and a_2 are semi-axes, but a_3 is the third semi-axis only in the limit $d \to 0$. The true third semi-axis is z_M, i.e., the solution of the equation

$$\frac{z^2}{a_3^2}+d\,\frac{z^4}{a_3^4}=1, \tag{2}$$

that is,

$$z_M=\frac{a_3}{\sqrt{2}}\sqrt{\frac{\sqrt{1+4\,d}}{d}-\frac{1}{d}}. \tag{3}$$

Following (Jeans 1919) the distorted ellipsoids will be called ellipsoidal figures, rather than ellipsoids. In order for the figures to be closed, z_M must be a real number, i.e. d is limited to

$$d \geq -\frac{1}{4}. \tag{4}$$

According to equation (3) a_3 can be eliminated from equation (1) in terms of the true semi-axis z_M, but this would be impractical.

3. THE GRAVITATIONAL POTENTIAL OF THE HETEROGENEOUS BODY

The body's atmosphere total potential at an interior point is composed of two contributions: an interior one, coming from the whole body, assumed to have a density ρ_a throughout, and an exterior one, coming from a hypothetical nucleus of density $\rho_n-\rho_a$, which compensates the mass excess of the former calculation; similarly, the nucleus total potential is composed of two interior contributions. On the other hand, the confocality condition, which helped to render straightforward the evaluation of the potential (Lyttleton 1953; Macmillan 1958) in our past models, is no longer useful; in fact, as we shall see in our next paper, the nucleus and atmosphere of our current heterogeneous model are *similar* ellipsoidal figures, rather than confocal.

In general, the potential of a continuous mass of density ρ, at a point (x_1, x_2, x_3), is given by (Thornton & Marion 2008)

$$V=G\rho\int\frac{d\tau}{R}, \tag{5}$$

where G is the gravitational constant, $R=\sqrt{(x-x_1)^2+(x-x_2)^2+(x-x_3)^2}$ and $d\tau$ is the volume element. Also needed are the derivatives of V:

$$\frac{\partial V}{\partial x_1}=G\rho\int\frac{d\tau}{R^3}\,(x-x_1),\quad \frac{\partial V}{\partial x_2}=G\rho\int\frac{d\tau}{R^3}\,(y-x_2),\quad \frac{\partial V}{\partial x_3}=G\rho\int\frac{d\tau}{R^3}\,(z-x_3). \tag{6}$$

Taking the field point (x_1,x_2,x_3) as the origin of spherical coordinates (R,ϑ,φ), where R is the distance from that point to the source point (x,y,z), and using the relations connecting spherical and rectangular coordinates, namely,

$$x=x_1+R\sin\vartheta\cos\varphi,\quad y=x_2+R\sin\vartheta\sin\varphi,\quad z=x_3+R\cos\vartheta, \tag{7}$$

the potential V and its derivatives become

$$V=\frac{1}{2}\,\rho\int_\vartheta\int_\varphi[R_2^2(\vartheta,\varphi)-R_1^2(\vartheta,\varphi)]\sin\vartheta d\vartheta d\varphi, \tag{8}$$

$$\frac{\partial V}{\partial x_1}=\rho\int_\vartheta\int_\varphi[R_2(\vartheta,\varphi)-R_1(\vartheta,\varphi)]\sin^2\vartheta\cos\varphi\,d\vartheta\,d\varphi, \tag{9}$$

$$\frac{\partial V}{\partial x_2}=\rho\int_\vartheta\int_\varphi[R_2(\vartheta,\varphi)-R_1(\vartheta,\varphi)]\sin^2\vartheta\sin\varphi\,d\vartheta\,d\varphi, \tag{10}$$

$$\frac{\partial V}{\partial x_3}=\rho\int_\vartheta\int_\varphi[R_2(\vartheta,\varphi)-R_1(\vartheta,\varphi)]\sin\vartheta\cos\vartheta\,d\vartheta\,d\varphi. \tag{11}$$

where we have omitted (as we will do hereinafter) the constant G; here, $R_2(\vartheta,\varphi)$, and $R_1(\vartheta,\varphi)$, are the two positive solutions of the equation

$$\frac{(x_1+R\sin\vartheta\cos\varphi)^2}{a_1^2}+\frac{(x_2+R\sin\vartheta\sin\varphi)^2}{a_2^2}+\frac{(x_3+R\cos\vartheta)^2}{a_3^2}+d\,\frac{(x_3+R\cos\vartheta)^4}{a_3^4}=1. \tag{12}$$

For an exterior point, R_2 and R_1 correspond to the body's surface points (for a given pair (ϑ,φ)) where R cuts it; for an interior point there is only one intersection, so that $R_1=0$ and $R_2\neq 0$. Equation (12) must be solved for each (x_1,x_2,x_3). For an interior point, the limits of ϑ, and φ are simply $(0,\pi)$, and $(0,2\pi)$, respectively, but for an exterior point the limits are more complicated.

3.1. *Limits of ϑ and φ for exterior points*

It should be realized that in going from an exterior point to any point on the body's surface, the angle ϑ cannot take any value within the range $0<\vartheta<\pi$, because it is restricted by the limits arising from all the tangents to the surface that can be drawn from the point, thus generating a cone with vertex at (x_1,x_2,x_3); r is constrained to vary only inside this cone. The loci of the tangent points (x,y,z) are given by equation (1), and the relation

$$(x_1-x)\,\frac{x}{a_1^2}+(x_2-y)\,\frac{y}{a_2^2}+(x_3-z)\,\frac{z}{a_3^2}+2\,d\,(x_3-z)\,\frac{z^3}{a_3^4}=0, \tag{13}$$

that is, two of the coordinates are determined as a function of the third. For the sake of simplicity, z will be taken as the independent variable (parameter). Solving the equations, two z-dependent solutions are obtained:

$$x_{11}=\frac{a_1^2a_2^2a_3^4x_1\left(a_3^4-a_3^2x_3z+dz^3(-2x_3+z)\right)-\sqrt{r_a}}{a_3^8\,(a_2^2x_1^2+a_1^2x_2^2)},$$

$$y_1=\frac{a_2^2\left(a_1^4a_3^4x_2^2\left(a_3^4-a_3^2x_3z+dz^3(-2x_3+z)\right)+x_1\sqrt{r_a}\right)}{a_1^2a_3^8\,(a_2^2x_1^2x_2+a_1^2x_2^3)},$$

$$x_{12}=\frac{a_1^2a_2^2a_3^4x_1\left(a_3^4-a_3^2x_3z+dz^3(-2x_3+z)\right)+\sqrt{r_a}}{a_3^8\,(a_2^2x_1^2+a_1^2x_2^2)},$$

$$y_2=\frac{a_2^2\left(a_1^4a_3^4x_2^2\left(a_3^4-a_3^2x_3z+dz^3(-2x_3+z)\right)-x_1\sqrt{r_a}\right)}{a_1^2a_3^8\,(a_2^2x_1^2x_2+a_1^2x_2^3)},$$

where the radicand r_a is given by

$$r_a = -a_1^4 a_3^8 x_2^2 \left[a_2^2 a_3^4 x_1^2 \left(-a_3^4 + a_3^2 z^2 + dz^4\right) + a_1^2 \left[a_3^4 x_2^2 \left(-a_3^4 + a_3^2 z^2 + dz^4\right) + a_2^2 \left(a_3^4 - a_3^2 x_3 z + dz^3(-2x_3 + z)\right)^2\right]\right]. \tag{14}$$

For some very special (singular) situations, the solution may differ from the above, but this point will not concern us. We require real solutions in order to have physically meaningful results, and so $r_a \geq 0$. The r_a limit for having real roots is $r_a = 0$, thereby resulting two extremes values, let us call them z_a and z_b, that must lie in the range $(-z_M, z_M)$. With the points (x_{11}, y_1, z), one half of the tangent curve can be built if z is let to run from z_a to z_b, while the other half comes from the points (x_{12}, y_2, z). Letting z vary in its allowed range, the angles ϑ and φ change from a minimum value to a maximum, which can be found with the expressions

$$\varphi = \arctan \frac{y_1 - x_2}{x_{11} - x_1}, \quad \vartheta = \arccos \frac{z - x_3}{R}, \tag{15}$$

$$R = \sqrt{(x_1 - x_{11})^2 + (x_2 - y_1)^2 + (x_3 - z)^2},$$

and

$$\varphi = \arctan \frac{y_2 - x_2}{x_{12} - x_1}, \quad \vartheta = \arccos \frac{z - x_3}{R'}, \tag{16}$$

$$R' = \sqrt{(x_1 - x_{12})^2 + (x_2 - y_2)^2 + (x_3 - z)^2}.$$

According to these equations, the spherical angles are functions of z: $\vartheta = \vartheta(z)$ and $\varphi = \varphi(z)$, so that after eliminating z we have

$$\vartheta = \vartheta(\varphi). \tag{17}$$

It is found that for each φ there are two ϑ values: ϑ_1 and ϑ_2. Therefore, the integration limits of the integrals (8)-(11) for exterior points are:

$$\vartheta = (\vartheta_1(\varphi), \vartheta_2(\varphi)), \qquad \varphi = (\varphi_a, \varphi_b), \tag{18}$$

where φ_a and φ_b are the maximum and minimum values that φ can take.

4. THE EQUILIBRIUM EQUATIONS AND A NORMALIZATION

Each fluid particle of our model, while subjected to the whole body's gravitational field, moves about the z-axis with a certain velocity $\mathbf{v}$; thence its equation of motion is

$$\frac{d}{dt}\left(V + \frac{p}{\rho} + \frac{1}{2}v^2\right) = \frac{\partial}{\partial t}\left(V + \frac{p}{\rho}\right), \tag{19}$$

where p is the pressure at the point. Our concern is aimed at a steady state and so the right-hand side of this equation is zero, that is,

$$V + \frac{p}{\rho} + \frac{1}{2}v^2 = \text{cte.}; \tag{20}$$

i.e., Bernoulli's theorem (Dryden 1956), which holds for any streamline, will be the governing 'equilibrium' equation of our body.

The dimensions of the masses under study are typically of order 10^9 m; it is possible to avoid dealing with such inconvenient quantities if the semi-axes are normalized—as will be implicit hereinafter—taking a_1 as a scale factor. For the surface coordinates we write

$$x = a_1\, x', \quad y = a_1\, y', \quad z = a_1\, z', \tag{21}$$

for the reference point

$$x_1 = a_1\, x_1', \quad x_2 = a_1\, x_2', \quad x_3 = a_1\, x_3', \tag{22}$$

and for the potential and its derivatives

$$V = a_1^2 \rho\, V', \quad \frac{\partial V}{\partial x_1} = a_1 \rho\, \frac{\partial V'}{\partial x_1'}, \quad \frac{\partial V}{\partial x_2} = a_1 \rho\, \frac{\partial V'}{\partial x_2'}, \quad \frac{\partial V}{\partial x_3} = a_1 \rho\, \frac{\partial V'}{\partial x_3'}, \tag{23}$$

The normalized surface equation takes the form

$$x^2 + \frac{y^2}{e_2^2} + \frac{z^2}{e_3^2} + d\,\frac{z^4}{e_3^4} = 1, \tag{24}$$

where $e_2 = a_2/a_1$, and $e_3 = a_3/a_1$; for economy of writing the normalized variables will be renamed as the original ones.

The equilibrium equation (20), which we write more explicitly farther on as equation (26), was found impossible to satisfy for a constant angular velocity, so this kind of motion had to be discarded. It seemed wise to replace it by an internal motion of non-uniform vorticity; the figures of our interest are therefore static, as seen from an inertial frame of reference. A moving fluid particle will describe an ellipse perpendicular to the z-axis, with the ellipse staying fixed in space, its axes pointing permanently along fixed directions.

Now, according to Dedekind, the vorticity $\boldsymbol{\zeta}$ of the ellipsoid internal motion is related to the rotation angular velocity $\boldsymbol{\omega}$ of the congruent Jacobi ellipsoid by (Chandrasekhar 1969)

$$\boldsymbol{\omega} = -\boldsymbol{\zeta}\,\frac{e_2}{1+e_2^2}, \qquad \text{or} \qquad \boldsymbol{\zeta} = -\boldsymbol{\omega}\,\frac{1+e_2^2}{e_2}, \tag{25}$$

$$\boldsymbol{\omega} = (0,0,\omega), \qquad \boldsymbol{\zeta} = (0,0,\zeta),$$

where $\boldsymbol{\omega}$ and $\boldsymbol{\zeta}$ are vectors along the z-axis: $\boldsymbol{\omega} = (0,0,\omega)$, and $\boldsymbol{\zeta} = (0,0,\zeta)$. Hereinafter, the term "angular velocity" will be used as synonymous to vorticity.

5. THE HOMOGENEOUS ELLIPSOIDAL MASS

So far, some of our considerations have been addressed to an inhomogeneous body; we wish, however, to adjourn this more general model for a future paper, and explore here only the case when no atmosphere is present; for, as we shall see, our homogeneous figures have some novel features which contrast with Jacobi's (or Dedekind's). The velocity of a rotating fluid particle is $\mathbf{v} = \omega(-y, x, 0)$.

5.1. *The equilibrium equations*

Since the body is self-gravitating, the pressure must vanish at each point on its bounding surface, so that equation (20) becomes

$$\rho\, V + \frac{1}{2}\,\rho\,\omega^2(x_1^2 + x_2^2) = \text{const.};$$

or, in terms of the normalized semi-axes

$$V + \Omega\,(x_1^2 + x_2^2) = k, \qquad \Omega = \frac{\omega^2}{2a_1\rho G}, \tag{26}$$

(x_1, x_2, x_3) are the coordinates of a surface point where the potential has to be evaluated, in order to satisfy this boundary condition. As we have pointed out, equation (26) cannot be satisfied for a constant angular velocity, contrasting with Jacobi's figures, for which the angular velocity is constant at all body's surface points, for a given pair of eccentricities. We will assume that the angular velocity (vorticity) depends on the coordinates of the point, the dependence being restricted only by the continuity equation $\mathbf{div}\ \mathbf{v} = 0$; that is,

$$\frac{\partial \omega}{\partial x_1^2} = \frac{\partial \omega}{\partial x_2^2},$$

from which we infer that

$$\omega = \omega(r, x_3), \quad \text{and} \quad \Omega = \Omega(r, x_3), \qquad r = x_1^2 + x_2^2. \tag{27}$$

By totally differentiating equation (26) and using the surface equation (equation 24), there result the following two expressions

$$2\left(1 - e_2^2\right)\Omega + 2\left(1 - e_2^2\right) r\frac{\partial \Omega}{\partial r} + b_1 - e_2^2 b_2 = 0, \tag{28}$$

$$-2\Omega - 2r\frac{\partial \Omega}{\partial r} + \frac{e_3^2 r}{d_3 e_2^2 x_3}\frac{\partial \Omega}{\partial x_3} - b_2 + \frac{e_3^2}{d_3 e_2^2} b_3 = 0, \tag{29}$$

where we have written

$$b_1 = \frac{1}{x_1}\frac{\partial V}{\partial x_1}, \quad b_2 = \frac{1}{x_2}\frac{\partial V}{\partial x_2}, \quad b_3 = \frac{1}{x_3}\frac{\partial V}{\partial x_3}, \quad d_3 = 1 + \frac{2dx_3^2}{e_3^2}.$$

For the special case in which $d = 0$ and b_i and Ω are constants, equations (28) and (29) become

$$2(1 - e_2^2)\,\Omega + b_1 - e_2^2\, b_2 = 0, \qquad -2\Omega - b_2 + \frac{e_3^2}{e_2^2} b_3 = 0, \tag{30}$$

which are the classical equilibrium conditions for Jacobi's figures.

At the pole ($r = 0$) the equilibrium conditions (26), (28) and (29) become

$$k = V_p, \tag{31}$$

$$2(1 - e_2^2)\,\Omega_p + b_{1p} - e_2^2\, b_{2p} = 0, \tag{32}$$

$$-2\Omega_p - b_{2p} + \frac{e_3^2}{d_3 e_2^2} b_{3p} = 0, \qquad x_3 = z_M, \tag{33}$$

where the subindex p refers to quantities pertaining to the pole.

5.2. *Results*

In this paper we are exclusively concerned about the existence of equilibrium figures; the question of stability, particulary about the possible presence of bifurcation points, i.e., the occurring of neutral frequencies, will be deferred to a next paper.

We may characterize one of our figures of fixed d by the quantities e_2, z_M (or e_3) and the angular velocity distribution $\Omega(r, x_3)$. The standard procedure for obtaining Jacobi's figures is to fix e_2 and then use equations (30) to settle e_3 and Ω. In our case, we can determine e_3 by fixing e_2 in equation (32), but this yields only Ω_p, the additional required quantity being the whole angular velocity $\Omega(r, x_3)$, which can be evaluated by an approximation method. We assume that, along a path (streamline) followed by a particle, the angular velocity is a linear function of r, say, $\Omega = \alpha_x + \alpha_y r$, where α_x, and α_y, are constants which can change from path to path (i.e., for different x_3 values), so that

$$\Omega(r, x_3) = \alpha_x(x_3) + \alpha_y(x_3)\, r. \tag{34}$$

Because of the implied tri-planar symmetry, the equilibrium equation for constant x_3, namely

$$V_p - V = \alpha_x\, r + \alpha_y\, r^2,$$

need to be solved only in the positive quadrant, for which a fitting procedure involving ten points will be employed. Each quarter of a meridian (i.e., the interval $[0, z_M]$) is divided into ten equidistant points, plus two

TABLE 1

SEMI-AXES ($a_1 = 1$) e_2, z_m, POLAR ANGULAR VELOCITY Ω_p, AND POLAR POTENTIAL V_p, FOR $d = 1/8$

e_2	e_3	z_M	Ω_p	V_p
0.99	0.6574037	0.623314	0.6107413	3.394020
0.95	0.6437333	0.610414	0.6101262	3.255665
0.90	0.6257421	0.593354	0.6080722	3.080440
0.80	0.5864383	0.556084	0.5987912	2.722499
0.70	0.5420833	0.514025	0.5807111	2.355015
0.60	0.4918012	0.466346	0.5509603	1.979067
0.50	0.4345488	0.412057	0.5058888	1.596755
0.40	0.3691012	0.349997	0.4410814	1.212036
0.30	0.2940654	0.278845	0.3518685	0.832397
0.20	0.2079810	0.197216	0.2355074	0.472689
0.10	0.1096994	0.104021	0.0993468	0.165242
0.05	0.0560198	0.053120	0.0359555	0.053368

backing points at the extremes, and the constants α_x and α_y are then evaluated for each path. Unfortunately the results so obtained contain an additional constant which is not small enough (especially near the equator), by which we mean quantities of order 10^{-7}; this is because V was determined with an accuracy no less than 10^{-7}. Therefore, equation (34) must be revised, for which purpose we set

$$\Omega(r, x_3) = \alpha_x(x_3) + \alpha_y(x_3)\, r + \frac{\alpha_s(x_3)}{r}, \quad \text{with} \quad \alpha_s(z_M) = 0, \tag{35}$$

so that Bernoulli's equation now reads

$$V_p - V = \alpha_s + \alpha_x\, r + \alpha_y\, r^2, \tag{36}$$

and the constants α_x, α_y and α_s can be evaluated in a similar fashion. Except near the equator, the new precision turns out to be much better than with $\alpha_s = 0$. Once the α parameters for each path of a specific figure have been evaluated, the corresponding angular velocity distribution follows.

Notice that for every d value there corresponds a series, each characterized by the various possible semi-axes, and the corresponding angular velocity distributions. As is well-known, for $d = 0$ the Jacobi series follows, which admits only a pair of axes for any angular velocity value.

We may obtain one of our series by fixing e_2 in equations (32) and (33) and solving them for e_3 and Ω_p, thus determining the possible semi-axes. Table 1 gives data for $d = 1/8$. Table 1 shows that beginning at 0.6107 where the largest polar angular velocity occurs (and where the figure is nearly spheroidal), the semi-axes e_2 and z_M continuously decrease with decreasing Ω_p, just as observed in Jacobi's ellipsoids. From $e_2 \simeq z_M = 0.1$ on, the situation reverses and we have $z_M \gtrsim e_2$ (not observed in Jacobi's figures); this last behavior will later be discussed. Next, the figure's angular velocity distribution must be determined, for which we proceed as explained above. Table 2 summarizes the results for $e_2 = 0.5$ (seventh row of Table 1), and Figure 1 is the corresponding plot of Ω vs. r.

According to Figure 1 the path's angular velocity with $x_3 = \text{const.}$ decreases from the major axis (r large) to the e_2-axis (smaller r). In addition, a global tendency of the angular velocity to decrease from the pole to the equator can be inferred, since α_x and α_y themselves decrease.

Since Table 2 is not particularly suitable for practical situations, we will try to describe our results with somewhat more clarity by empirically establishing analytical expressions. Due to our limited computation

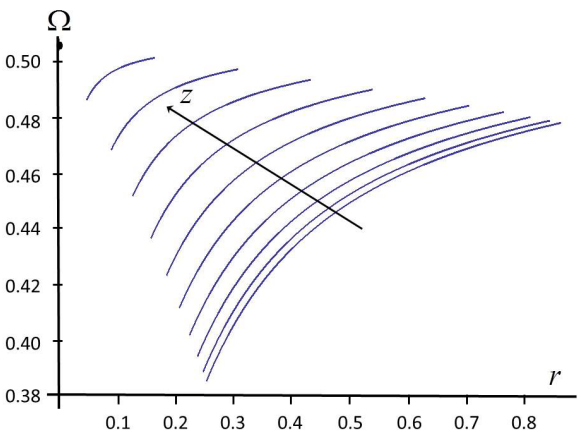

Fig. 1. Angular velocity distribution in an ellipsoidal figure with $d = 1/8$, $e_2 = 0.5$ and $z_M = 0.4121$. Each curve gives the angular velocity as a function of r for a trajectory $z = x_3 = \text{const.}$. The bottom curve corresponds to one fourth of the equator, and the topmost (thick point) to the pole.

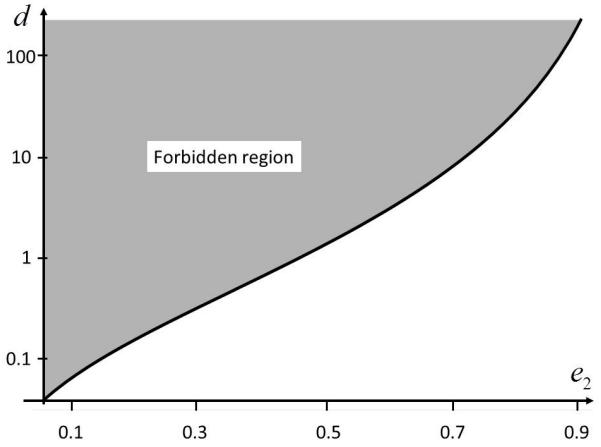

Fig. 2. The limiting d-curve points are characterized by the property $z_M = e_2$. The forbidden region corresponds to figures with $z_M > e_2$. The curve is plotted using a logarithmic scale for d.

TABLE 2

ANGULAR VELOCITY PARAMETERS $\Omega = \alpha_x + \alpha_y\, r + \alpha_s/r$ AS FUNCTION OF CONTOUR LEVEL, x_3, FOR $e_2 = 0.5$ (7TH ROW OF TABLE 1)[a]

x_3	α_x	α_y	α_s
0.0374559	0.5125501	0.0038054	-0.0325523
0.0749119	0.5123801	0.0037891	-0.0309362
0.1123678	0.5120970	0.0037621	-0.0283352
0.1498238	0.5117015	0.0037250	-0.0248876
0.1872797	0.5111943	0.0036781	-0.0207866
0.2247357	0.5105765	0.0036222	-0.0162794
0.2621916	0.5098497	0.0035580	-0.0116667
0.2996476	0.5090153	0.0034864	-0.0073021
0.3371035	0.5080754	0.0034083	-0.0035906
0.3745595	0.5070323	0.0033245	-0.0009880

[a]The error in k (equation (26)), due to the approximation in Ω, is less than about 10^{-6}.

facilities, we tried not to spend too much time seeking an optimal fit. We found that the parameters α_x, α_y and α_s as given by

$$\alpha_x = \alpha_{x0} + \alpha_{x1}\, x_3^2, \qquad \alpha_y = \alpha_{y0} + \alpha_{y1}\, x_3^2, \qquad \alpha_s = \alpha_{s0}\, z_s + \alpha_{s1}\, z_s^2, \tag{37}$$

with

$$z_s = \left(1 - \frac{x_3^2}{e_3^2} - d\,\frac{x_3^4}{e_3^4}\right)(z_M - x_3)\,, \tag{38}$$

reproduce the angular velocity with an uncertainty at about the fifth decimal place (for larger d the uncertainty can be in the second decimal place). In this way, the angular velocity distribution based on Table 2 is

TABLE 3

PARAMETERS OF THE ANGULAR VELOCITY $\Omega = \alpha_{x0} + \alpha_{x1}\, x_3^2 + (\alpha_{y0} + \alpha_{y1}\, x_3^2)\, r + (\alpha_{s0}\, z_s + \alpha_{s1}\, z_s^2)/r$, AS A FUNCTION OF e_2 AND z_M

e_2	z_M	α_{x0}	α_{x1}	α_{y0}	α_{y1}	α_{s0}	α_{s1}
0.99	0.623314	0.619643	-0.023107	0.002463	-0.001061	-0.207990	0.136757
0.95	0.610353	0.619016	-0.024067	0.002562	-0.001148	-0.203685	0.136770
0.90	0.593294	0.616919	-0.025348	0.002692	-0.001272	-0.198056	0.136812
0.80	0.556029	0.607437	-0.028204	0.002967	-0.001581	-0.185878	0.137003
0.70	0.513974	0.588967	-0.031512	0.003256	-0.002004	-0.172291	0.137377
0.60	0.466299	0.558587	-0.035347	0.003546	-0.002601	-0.157013	0.137996
0.50	0.412015	0.512595	-0.039771	0.003804	-0.003483	-0.139678	0.138936
0.40	0.349962	0.446541	-0.044795	0.003963	-0.004861	-0.119798	0.140297
0.30	0.278817	0.355768	-0.050245	0.003892	-0.007211	-0.096719	0.142188
0.20	0.197196	0.237672	-0.055378	0.003340	-0.011841	-0.069582	0.144671
0.10	0.104011	0.099982	-0.057267	0.001921	-0.024017	-0.037413	0.147578
0.05	0.053115	0.036114	-0.052974	0.000846	-0.041463	-0.019265	0.148972

approximately described by

$$\Omega = (0.51260 - 0.03977\, x_3^2) + (0.00380 - 0.00348\, x_3^2)\, r + \frac{\text{-}0.13968\, z_s + 0.13894\, z_s^2}{r}. \tag{39}$$

With this angular velocity expression the complete set of figures based on Table 1 can be obtained, which we list in Table 3.

5.3. *The forbidden ellipsoidal figures*

Our ellipsoidal figures have semi-axes 1, e_2 and z_M, the last being for a fixed e_2 a measure of the flattening: as z_M decreases the figures become more flattened. According to our calculations, in equilibrium conditions the parameter d in the figure's equation determines z_M. Fixing e_2 at some intermediate value, say, 0.5, we now inquire about the effect on z_M as d increases, starting at its minimum value $-1/4$, thus constructing Table 4. The d range can be split into two segments: from $d = -1/4$ to $d = 1.37576$ corresponding to figures with $z_M \leq e_2$ (or figures of high flattening); and for $d > 1.37576$, which characterize figures with $z_M \geq e_2$ (or figures of low flattening). In this last case z_M is not the smallest axis, but e_2. The segment $-1/4 < d < 1.37576$ can further be divided from $-1/4$ to 0 and from 0 to 1.37576, the first (second) comprises figures more (less) flattened than Jacobi's ellipsoids. The figures with e_2 as the smallest axis are not physically acceptable because by equation (36) Ω ($\sim \omega^2$) must necessarily be negative, since near the e_2-axis we have $V > V_p$. This region in the d-e_2 plane is therefore forbidden for our figures.

We now derive the relation $d = d(e_2)$ for which $z_M = e_2$. For this purpose, we build a table similar to Table 1 varying e_2 and determining d and Ω_p instead of e_3 and Ω_p. These results are summarized in Table 5, and Figure 2 is a logarithmic plot of d vs. e_2. Figure 2 shows the limiting d-curve that separates the region of allowed equilibrium figures ($z_M < e_2$) from that of physically impossible ones ($z_M > e_2$; shaded area); for a given d and e_2, a series of figures starting upwards at this e_2 value can be obtained. Thus, as d increases, so does e_2, and the series becomes narrower. The Jacobi series, which corresponds to $d = 0$ and starts at $e_2 = 0$ is accordingly the widest series.

One interesting aspect of the frontier figures is that the angular velocity vanishes at point $(0, e_2, 0)$ on the equator, i.e. the particle is momentarily at rest there. For example, for the limiting figure with $e_2 = 0.5$, and $d = 1.3757$, the angular velocity distribution is as shown in Figure 3. In Figure 3, each contour represents Ω as a function of the squared distance r to the rotation axis; the lower one corresponds to the equator ($x_3 = 0$), for which $\Omega = 0$ at $r = 0.25$.

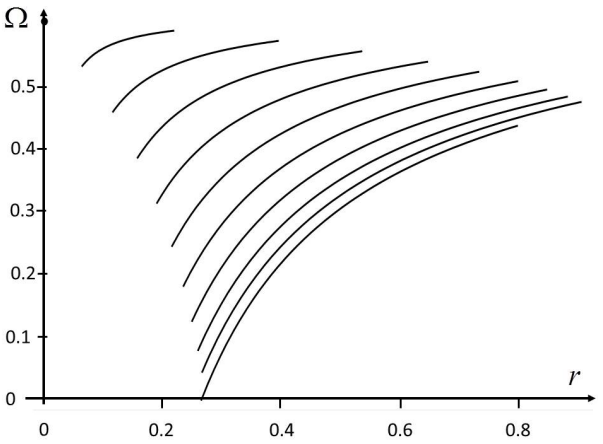

Fig. 3. Ω-distribution on the frontier figure surface with $e_2 = 0.5$ and $d = 1.3757$. Each curve corresponds to a level $x_3 = \text{const.}$, the lower refers to the 4th of the equator. This curve has $\Omega = 0$ at $r = 0.25$.

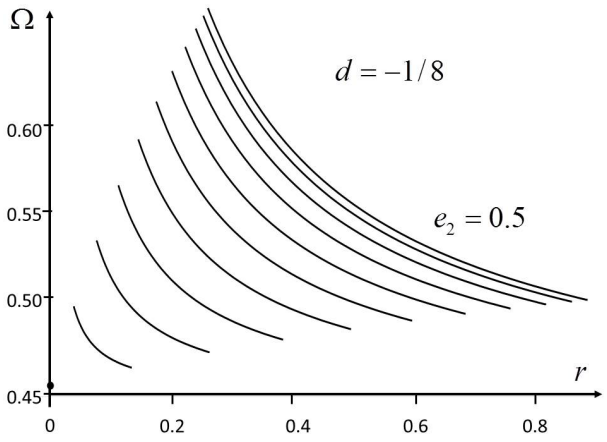

Fig. 4. Ω-distribution on the surface of the figure with $e_2 = 0.5$ and $d = -1/8$.

TABLE 4

SEMI-AXIS z_M AND ANGULAR VELOCITY Ω_p AT THE POLE[a]

d	e_3	z_M	Ω_p
-0.24	0.121315	0.156617	0.267996
-0.20	0.223374	0.262592	0.384846
-0.10	0.325414	0.345463	0.457815
0.10	0.425481	0.407237	0.502733
0.20	0.459227	0.424407	0.513867
0.30	0.487629	0.437618	0.522053
0.40	0.512306	0.448249	0.528403
0.50	0.534218	0.457076	0.528403
0.60	0.553989	0.464578	0.537754
0.70	0.572047	0.471067	0.541337
0.80	0.588699	0.476762	0.544420
0.90	0.604175	0.481819	0.547111
1.00	0.618649	0.486352	0.549485
1.37576	0.666157	0.500001	0.556423
2.00	0.729067	0.515528	0.563938
7.00	0.999921	0.559622	0.583197

[a]The values are given as a function of d, for $e_2 = 0.5$. e_3 is included as a byproduct.

TABLE 5

SEMI-AXIS e_2, d AND THE ANGULAR VELOCITY Ω_p AT THE POLE[a]

e_2	e_3	d	Ω_p
0.90	6.2003630	220.49916	0.7200396
0.80	1.9499815	29.354738	0.6984864
0.70	1.2614507	7.2978365	0.6659624
0.60	0.9048244	2.8974497	0.6196744
0.50	0.6661618	1.3757080	0.5564224
0.40	0.4856688	0.6990221	0.4728749
0.30	0.3388724	0.3520459	0.3664056
0.20	0.2134747	0.1586715	0.2374685
0.10	0.1022864	0.0483855	0.0969456

[a]For completeness e_3 is included.

The reason for obtaining models with $\Omega < 0$ is because, contrary to what ordinarily occurs, the maximum of the potential does not occur at the pole, but right on the e_2-axis, at the point $(0, e_2, 0)$. We might attempt to rescue forbidden models if the constant k in equation (26) is taken as the maximum potential, instead of V_p; in this way, negative values of $V_{\max} - V$ would be avoided and hence $\Omega \geq 0$; however, this would imply $\Omega = \infty$ at the pole, since $\alpha_s = V_{\max} - V_p$.

TABLE 6

SEMI-AXIS z_M AND PARAMETERS OF THE APPROXIMATE ANGULAR VELOCITY $\Omega = \Omega_0 + \Omega_1 x_3^2 + \Omega_2 x_3^4 + \Omega_3 x_3^6$ [a]

		$\Omega = \Omega_0 + \Omega_1\, x_3^2 + \Omega_2 x_3^4 + \Omega_3 x_3^6$			
z_M	Ω_p	Ω_0	Ω_1	Ω_2	Ω_3
0.623314	0.6107413	0.619642	-0.023106	0.002462	-0.001060
0.610414	0.6101262	0.619015	-0.024067	0.002562	-0.001148
0.593354	0.6080722	0.616918	-0.025347	0.002691	-0.001272
0.556084	0.5987912	0.607437	-0.028203	0.002966	-0.001580
0.514025	0.5807111	0.588967	-0.031512	0.003256	-0.002003
0.466346	0.5509603	0.558587	-0.035346	0.003546	-0.002601
0.412057	0.5058888	0.512595	-0.039771	0.003804	-0.003482
0.349997	0.4410814	0.446540	-0.044794	0.003963	-0.004861
0.278845	0.3518685	0.355768	-0.050244	0.003891	-0.007211
0.197216	0.2355074	0.237672	-0.055377	0.003339	-0.011841
0.104021	0.0993468	0.099981	-0.057267	0.001921	-0.024016
0.053120	0.0359555	0.036113	-0.052974	0.000845	-0.041463

[a]The values given correspond to the spheroidal figures of the series with $d = 1/8$; the pole's angular velocity Ω_p is included (second column).

The figures for negative d (from 0 to $-1/4$), have the following peculiarity. As was previously remarked, figures with negative d are more flattened than those with $d > 0$; in addition, the angular velocity distribution becomes, in a certain sense, reversed, since Ω increases from the pole to the equator—rather than the opposite—; Figure 4 is a plot of Ω vs. r, for $d = -1/8$ and $e_2 = 0.5$ (to be compared with Figure 1).

6. THE SPHEROIDAL FIGURES

For the special case $e_2 = 1$, the path of a fluid particle will be a circle of radius $\sqrt{r}$, and we have spheroidal figures. The surface equation of the distorted spheroid is

$$x_1^2 + x_2^2 + \frac{x_3^2}{e_3^2} + d\,\frac{x_3^4}{e_3^4} = 1, \quad \text{or} \quad r + \frac{x_3^2}{e_3^2} + d\,\frac{x_3^4}{e_3^4} = 1. \tag{40}$$

By symmetry, the potential will depend only on r $(= x_1^2 + x_2^2)$ and x_3: $V = V(r, x_3)$. The angular velocity along a path of fixed x_3 will now be constant, and the equilibrium equations (28) and (29) reduce to

$$-2\Omega - 2r\frac{\partial \Omega}{\partial r} + \frac{e_3^2 r}{d_3 x_3}\frac{\partial \Omega}{\partial x_3} - b_1 + \frac{e_3^2}{d_3}\,b_3 = 0, \tag{41}$$

where

$$d_3 = 1 + \frac{2dx_3^2}{e_3^2};$$

assuming the r dependence like in equation (34), with α_y as stated in equation (37), Ω becomes a sixth-order even polynomial in x_3. Let us take

$$\Omega = \Omega_0 + \Omega_1 x_3^2 + \Omega_2 x_3^4 + \Omega_3 x_3^6, \tag{42}$$

where $\Omega_0, \ldots, \Omega_3$ are constants. The pole's angular velocity is determined by

$$-b_{1p} + \frac{e_3^2}{d_3}\,b_{3p} - 2\Omega_p = 0,$$

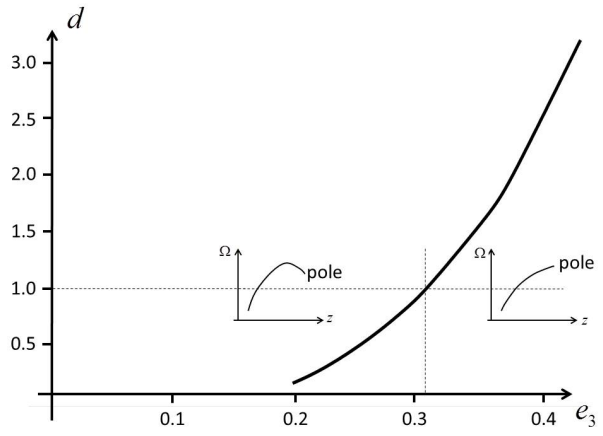

Fig. 5. Limiting d-curve that separates the region of Ω-distribution with a maximum at the pole from that with a maximum between pole and equator.

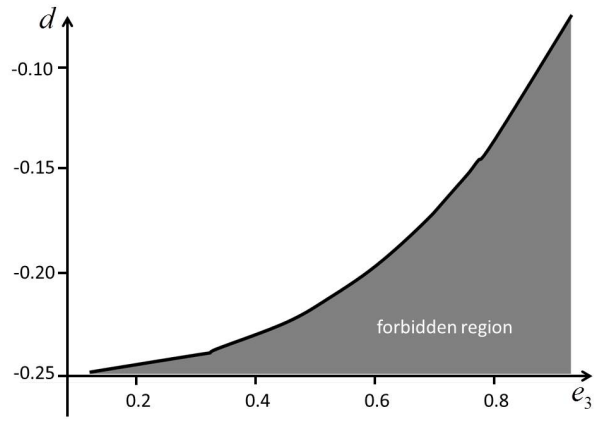

Fig. 6. d-curve in the range of negative values that separates spheroidal figures with $\Omega > 0$ from those with $\Omega < 0$ (shaded area).

and Bernoulli's equation becomes

$$V + r\left(\Omega_0 + \Omega_1 x_3^2 + \Omega_2 x_3^4 + \Omega_3 x_3^6\right) = V_p. \tag{43}$$

The determination of the Ω-constants can be achieved similarly as for the ellipsoidal figures, using again a quarter of a meridian. We calculate V at each point, and determine them by fitting equation (41) now with 16 supporting points; these results are summarized in Table 6.

TABLE 7

e_3, z_M, d

e_3	z_M	d
0.201936	0.191486	0.1250
0.225870	0.205603	0.2500
0.262716	0.224803	0.5000
0.291115	0.237719	0.7500
0.314471	0.247248	1.0000
0.351958	0.260707	1.5000
0.381815	0.270015	2.0000
0.042854	0.282426	3.0000

TABLE 8

SEMI-AXIS ($a_1 = 1$, $e_2 = 1$) z_M, e_3, d

e_3	z_M	d
0.100836	0.138297	-0.2490
0.137018	0.185648	-0.2480
0.278700	0.359500	-0.2400
0.307095	0.392615	-0.2375
0.412897	0.508969	-0.2250
0.488477	0.586509	-0.2125
0.548787	0.645138	-0.2000
0.599570	0.692323	-0.1875
0.643739	0.731777	-0.1750
0.683007	0.765636	-0.1625
0.718474	0.795253	-0.1500
0.737333	0.810635	-0.1428
0.750894	0.822539	-0.1375
0.780809	0.845142	-0.1250
0.904208	0.936105	-0.0625

For positive d, there are no restrictions as to the existence of spheroidal figures. However, the angular velocity distribution behaves according to two different patterns: in one, the maximum of Ω occurs somewhere between the equator and the pole; while in the other, it appears right at the pole; these results are summarized in Table 7, and Figure 5 is a plot of d vs. e_3, showing the boundary curve separating these two patterns. For a given d, for example $d = 1$, there is a value of e_3 (≈ 0.3), below which the first pattern shows up and above which the other pattern occurs.

6.1. *The forbidden spheroidal figures*

For negative d, there result figures with $\Omega < 0$, that must be discarded. Figure 6 is a plot of $-d$ vs. e_3, showing the curve that separates the region of forbidden figures (shaded area) from the permitted ones. For a given d value, for example $d = -0.2$, there corresponds a e_3 value (≈ 0.6) below which figures exist, but are physically impossible otherwise.

REFERENCES

Chandrasekhar, S. 1969 Ellipsoidal Figures Of Equilibrium (Yale: University Press)

Cisneros, J. U., Martínez, F. J., & Montalvo, J. D. 1983, RMxAA, 5, 293

Cisneros, J. U., Martínez, F. J., & Montalvo, J. D. 2000, RMxAA, 36, 185

Cisneros, J. U., Martínez, F. J., & Montalvo, J. D. 2004, RMxAA, 40, 167

Dryden, H. L., Murnaghan, F. P. & Bateman, H. 1956, Hydrodynamics (Dover Publications Inc.)

Hamy, M. 1887, Etude sur la Figure des Corps Célestes, Theśe de la Faculté des Sciences, Annales de l'Observatoire de Paris, 1889, Mémoires, 19

Jeans, J. H. 1919, PhilTrans.R.Soc., (Cambridge, England Cambridge University Press)

Lyttleton, R. A. 1953, The Stability of Rotating Liquid Masses (Cambridge: Cambridge University Press)

MacMillan, W. D. 1958, Theoretical Mechanics: The Theory of the Potential (New York: Dover Publications)

Montalvo, J. D., Martínez, F. J. & Cisneros, J. U. 1983, RMxAA, 5, 293

Tassoul, J. L. 1978, Theory of Rotating Stars, (Princeton: Princeton Univ. Press)

Joel U. Cisneros Parra: Facultad de Ciencias, Universidad Autónoma de San Luis Potosí, Zona Universitaria s/n, San Luis Potosí, S.L.P., México (cisneros@galia.fc.uaslp.mx).

Francisco J. Martínez Herrera and J. Daniel Montalvo Castro: Instituto de Física, Universidad Autónoma de San Luis Potosí, Zona Universitaria s/n, San Luis Potosí, S.L.P., México (marherrera@fciencias.uaslp.mx, montalvo@ifisica.uaslp.mx).